Evidence for three-dimensional flux creep in thin-film $Bi_2Sr_2CaCu_2O_{8+\delta}$

Goran Karapetrov and Janet Tate

Department of Physics and Center for Advanced Materials Research, Oregon State University
Corvallis, Oregon 97331-6507

We have measured sweep-rate dependent magnetization hysteresis curves of thin-film $Bi_2Sr_2CaCu_2O_{8+\delta}$ using a Hall probe magnetometer in an unconventional geometry. We find a structure in the response well below the three-dimensional to two-dimensional crossover field. The observed strong enhancement of the perpendicular field component's creep rate in the presence of an in-plane applied magnetic field is in contrast to recent findings. We attribute this to the existence of a finite correlation length between vortex pancakes along the field direction larger than the interlayer spacing leading to a three-dimensional behavior of flux lines in $Bi_2Sr_2CaCu_2O_{8+\delta}$ at 77 K.

INTRODUCTION

The discovery of high temperature superconductors (HTS's) triggered intensive experimental and theoretical investigation of their magnetic vortex structure, which differs significantly from that of their low temperature (LT) counterparts. First, the high critical temperature and short coherence lengths unveil large fluctuation effects which cannot be observed in LTS's. Second, their layered perovskite structure leads to large anisotropy of the superconducting carriers' effective mass $\gamma = (M/m)^{1/2}$ and consequently of all physical parameters which depend on it. In particular, the c-axis coherence length, whose ratio to the interplane distance d determines the strength of the coupling between the layers, becomes very short for large anisotropy. In this case, the phenomenological description of cuprates as a stack of superconducting layers coupled by the Josephson interaction seems appropriate.

The conventional concept of an Abrikosov vortex line lattice usually observed in LTS's breaks down at vanishing interlayer coupling strengths and a lattice of aligned two-dimensional (2D) vortex pancakes is formed instead.[1] This alters the static and dynamic magnetic response of the system because of a change in the interaction energy between the vortex lattice and the crystal as well as the interaction within the magnetic structure itself. Since in the pure 2D case (vanishing interlayer coupling) the superconducting critical current is supported only in the layers, the shielding is proportional to the perpendicular component of the magnetic field as observed early in magnetization and magnetic torque measurements.[2-4] On the other hand, if the interlayer correlation exceeds the interlayer spacing d but is smaller than the sample thickness t, the critical current should depend on the in-plane component of the magnetic field.[5]

The interesting dynamics of the vortex structure is in the angular region close to in-plane orientation of the applied magnetic field. This configuration, unstable in the limit of $\gamma \to \infty$, is stabilized by finite Josephson coupling between the layers. The magnetic field freely penetrates the interplane space forming a lattice of coreless Josephson vortices insensitive to the modulation of the order parameter along the c axis. Structural and dynamic changes in the vortex lattice organization have been predicted[6-8] and some of them experimentally observed.[9,10] Phase locking of such a lattice, described earlier by Feinberg and Villard[11] with a quantitative description by Bulaevskii et al.,[12] has been later observed in several sytems.[13-15]

The picture of the equilibrium flux line lattice (FLL) is changed in the presence of disorder that is always present in HTS's. Depending on the strength of disorder relative to the vortex line or pancake interaction, the properties of the FLL change significantly. Finite correlation lengths in this case force one to view the perfect vortex lattice as a form of a 3D or 2D vortex glass (VG) phase which eventually is destroyed by fluctuations. Destruction of the irreversibility is possible in several scenarios, depending on the parameters of the HTS material. Focusing on $Bi_2Sr_2CaCu_2O_{8+\delta}$ (BSCCO), with relatively weak disorder, it is more or less established that at fields larger than $B_{cr} \approx \frac{4\Phi_0}{(\gamma d)^2} \approx$ 1–10 kG, 2D melting of the VG by thermal fluctuations occurs when the shear modulus C_{66} and the tilt modulus C_{44} disappear at the same temperature.[16] In contrast, below B_{cr} melting is expected to be 3D: at some finite temperature, intraplane correlation is lost (C_{66} goes to zero) while the longitudinal correlation remains finite ($C_{44} > 0$) leading to finite tension of the vortex lines and therefore to their ability to be pinned by defects. As the temperature is raised further, the vortex lines lose their longitudinal order and evaporate into a gas of vortex pancakes. The low field aspect of this theoretical picture has been questioned by some authors[17,18] who contend that the temperature sequence of the elastic moduli disappearance is incorrect, and that two-dimensionality is already established well below 77 K.[19] This goes back to the question of the strength of the coupling between the superconducting layers compared to the vortex interaction within the plane and how susceptible that coupling is to thermal fluctuations and disorder.

The experiments testing the vortex structure in BSCCO in the nonequilibrium regime can be separated into two groups: those performed on as-grown samples and those dealing with crystals with artificially introduced columnar tracks. There has been no clear evidence so far for vortex lines in as-grown BSCCO samples. All physical properties have scaled with the perpendicular component of the applied magnetic field $H_a^\perp$.[20,2] Magnetic decoration experiments on as-grown BSCCO single crystals have shown that the static configuration of the flux lattice at 4 K in a tilted magnetic field depends only on $H_a^\perp$ (of course, decoration experiments probe the surface configuration of the flux lattice where the vortex-vortex interaction is different from the bulk). On the other hand, in irradiated crystals there has been evidence for unidirectional enhancement of pinning in a limited temperature range (above 50 K) suggesting that there exists a finite correlation between vortex pancakes along the field direction larger than d.[21,22] Since the irradiation significantly increases the vortex lines' tilt modulus, these experiments are not able to answer the question of what the "intrinsic" vortex structure is in this system, i.e., the one determined by the intrinsic properties of the sample.

In this paper we focus on an experimental investigation of the interaction between pinning centers and the FLL in an as-grown BSCCO thin film at 77 K in relatively weak magnetic fields below B_{cr}. We use an unconventional magnetic hysteresis loop (MHL) measurement of the magnetic moment projection onto the c axis of the film to probe the quasistatic response of the vortex lattice to applied fields swept through angles close to the superconducting planes. The results of our MHL measurements at low sweep rates show 3D behavior of the vortex lines — a strong dependence of the perpendicular field component's creep rate on the in-plane applied magnetic field for strongly tilted vortex lines.

EXPERIMENT

The high quality BSCCO thin film used in this experiment is c-axis oriented, 200 nm thick, on a $SrTiO_3$ (100) substrate, with a transition temperature of 87 K. The mosaic spread of the c-axis direction, determined from the width of the $(00\overline{1}0)$ rocking curve is about $0.4°$, and the Rutherford backscattering channeling minimum yield is 23%.[23] Scanning electron micrographs show a smooth surface with sub-micrometer-sized structures with a surface density of about $1/10$ μm^{-2}. We patterned the film into a 4.4-mm-diameter disk using wet etching photolithography. The boundary of the disk was smooth on a scale of 2 μm. The circular shape simplifies the calculation of electrodynamic quantities like critical current density and demagnetization factor.

Figure 1 shows the experimental setup for measuring the shielding currents induced in the film by the application of a time-varying magnetic field. The total field $\vec{H}_a^{tot}$ has two components: a static field $H_a^\parallel$ applied parallel to the Cu-O (ab) planes of the film, and a time-dependent component $H_a^\perp$ applied perpendicular to the
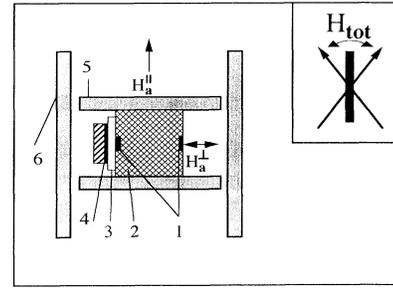

FIG. 1. Experimental setup: InSb Hall probes (1), sapphire sample holder (2), 0.5-mm MgO spacer (3), thin-film BSCCO disk (4), and a set of perpendicular solenoids (5,6).

planes. The angle of $\vec{H}_a^{tot}$ to the ab plane is Θ. The film's response to $H_a^\perp$ was determined by two InSb Hall probes positioned parallel to the film surface (so that the area vector is perpendicular to the film surface and parallel to $H_a^\perp$). One probe was separated from the center of the film by a 0.5-mm MgO spacer. It measured both the applied field $H_a^\perp$ and the response of the film. The other probe was about 30 mm from the film, far enough away not to detect the field generated by the shielding currents, but close enough that it measured the same applied field. Thus the difference in the signals directly gives the perpendicular component of $\vec{B}_{shield}$, the magnetic field generated by the shielding currents $\vec{J}_{shield}$ in the film. The field sensors, each with an active area of 100×100 μm^2 and a sensitivity of 2.75 μV/G at 50 mA driving current, were operated at 5 kHz to take advantage of lock-in recovery of the Hall voltage. We achieved a resolution of 1 mG$\sqrt{Hz}$. The magnetic field produced by the sensors and leads was too small to influence the results of the measurement.

The set of perpendicular solenoids which produce the two components of the applied field do not have significant flux linkage. This was verified by hysteresis measurements of the sample holder alone. The large outer solenoid that produces the static, in-plane field was operated between 0 and 150 Oe. The smaller, inner solenoid for the perpendicular component was swept between $\pm H_a^\perp \gg \pm H^*$, where H^* is the critical state field at the 77 K. The sweep rate $dH_a^\perp/dt$ could be varied from 0.2 to about 550 Oe/s, and was controlled with high accuracy by a function generator or an integrator at higher or lower sweep rates, respectively. This effectively rotated the applied field while keeping the projection in the ab plane constant. The magnitude of the applied field therefore changed as it rotated. For $H_a^\perp \approx$ 80 Oe and $H_a^\parallel \approx$ 150 Oe (the largest field), the field rotated about $28°$ on either side of the plane.

The Hall probes are parallel to the film substrate and perpendicular to $H_a^\perp$ to within $0.2°$. The solenoid producing the in-plane magnetic field is aligned with precision of $1°–2°$, and the in-plane field can be aligned exactly along the planes with a small dc offset in $H_a^\perp$. Consequently, only the irreversibility of the c-axis projection of the field created by the shielding currents is measured.

The entire experiment is in a variable temperature

cryostat, and the data presented here were generated at 77.4 K in a liquid nitrogen environment. We measured magnetization curves at several values of $H_a^{\parallel}$ and $dH_a^{\perp}/dt$ and extracted voltage-current (E-J) characteristics from them, along the lines suggested in Refs. 24–26. A more detailed discussion of the latter data analysis appears in the Appendix.

RESULTS

Figure 2 shows magnetization curves of a BSCCO thin film at 77 K at different sweep rates. There is no $H_a^{\parallel}$ component present so this corresponds to conventional measurements of superconductor response when the applied magnetic field is directed along the c axis and the magnetization component along the field direction is recorded. The amplitude of $H_a^{\perp}$ is 80 Oe and the shape of the magnetization curves indicates that the critical state is fully established.[27] The field dependence of the shielding currents derived from the width of the magnetization curves [Fig. 3] follows the exponential dependence observed in LTS's[28] as well as HTS's.[29] Considering the fact that, at this temperature, the in-plane penetration depth $\lambda_{ab} \approx 200$ nm is smaller than the average intervortex spacing $a_0 \approx (\Phi_0/B)^{1/2} \gtrsim 500$ nm, the vortex density is fairly dilute. Each vortex line interacts strongly with the underlying pinning centers and the intervortex interaction, although enhanced in the films,[30] is weaker than in the case of overlapping vortices.

The lowering of the sweep rate effectively lowers the threshold electric field E_c at which the critical current is measured. The shape of the irreversibility curves does not change significantly, although a large creep is evident. Derived E-J characteristics over four decades of electric field show the expected power law dependence associated with thermally activated flux creep in the current-dependent potential proposed by Zeldov et al.:[31]

$$U(j) = U_0 \ln(j_c/j) . \tag{1}$$

This describes thermally activated depinning of flux lines from potential wells with a triangular shape for $x \lesssim \xi$ and a logarithmic asymptote for $\xi < x < \lambda$. Linearity of the E-J curves on a log-log scale is evident for all $\mathrm{H}_a^{\perp}$, but the slope changes significantly from about 6.4 near
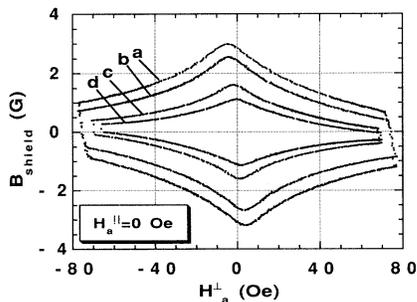

FIG. 2. Sweep-rate dependence of the magnetization curves at $H_a^{\parallel} = 0$ Oe: 445 (curve a), 131 (curve b), 4.7 (curve c), and 0.47 (curve d) Oe/s.
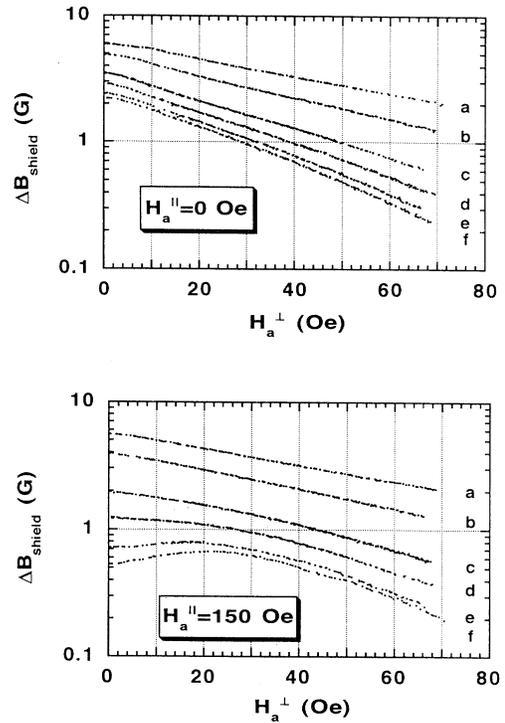

FIG. 3. Irreversibility of the shielding currents' field $\Delta B_{\mathrm{shield}}$ as a function of perpendicular applied magnetic field $H_a^{\perp}$ at different sweep rates $dH_a^{\perp}/dt$: 514 (curve a), 96.5 (curve b), 8.74 (curve c), 2.74 (curve d), 0.967 (curve e), 0.619 (curve f) Oe/s.

$H = 0$ G to 3.8 at higher fields. This corresponds to effective pinning potential energies[32] of 420 to 220 K.

Quite different behavior of the shielding current response is observed in the presence of a static magnetic field applied along the ab plane of the film. The magnitude of the in-plane field is of the order of the maximum $H_a^{\perp}$, so that varying $H_a^{\perp}$ can be viewed as a rotation of the total applied magnetic field vector about the ab plane within some angular range. If one assumes that at these temperatures and magnetic fields BSCCO with point disorder in the planes and weak coupling between the planes is quasi 2D, one does not expect any change in magnetization curves except perhaps for within the lock-in transition angular range. As is well known, the lock-in transition is suppressed in films[33] and it is destroyed by pinning disorder. Consequently, in this 2D picture, the irreversibility curves obtained in our case should not change in the presence of an in-plane magnetic field except for any changes in the pinning strength potential with total applied magnetic field.

That is what our experiment shows at high sweep rates. When the ramp rate $dH_a^{\perp}/dt$ decreases, a transformation of the shape of the irreversibility curves occurs. This is shown in Figs. 4 and 5. Figure 4 shows magnetization data at different sweep rates when a field of 150 Oe is applied parallel to the planes. First, small kinks in the magnetization appear near $H_a^{\perp} = 0$. They are not sym-
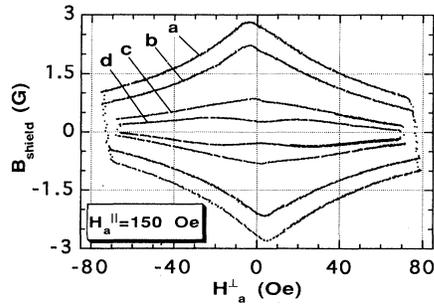
FIG. 4. Sweep-rate dependence of the magnetization curves at $H_a^{\parallel} = 150$ Oe: 445 (curve a), 131 (curve b), 4.7 (curve c), and 0.47 (curve d) Oe/s.

metric about the center. As the sweep rate decreases further, the kink develops into a minimum in the absolute magnetization at $H_a^{\perp} = 0$, and the curves become symmetric. At a given sweep rate the dip in magnetization is more pronounced if the in-plane field is larger (Fig. 5).

This anomaly is reminiscent of the "fishtail" or "peak effect"[34] observed in single crystals measured by conventional methods (projection of $\vec{M}$ along the direction of the applied field). Although the structure of the magnetization curves is similar we stress that there are subtle differences. First, the position of the maximum in $J_c(H)$ is an order of magnitude smaller in our case. Second, a peak effect has not been seen in HTS films. The similarity is that the anomaly becomes more pronounced with the applied field close to the ab plane.[35]

The enhanced dissipation near $H_a^{\perp} = 0$ leaves a clear footprint on the E-J characteristics (Fig. 6). At the point where the dip in the magnetization begins, $E(J)$ starts to deviate from power law dependence. For any $H_a^{\perp}$ between the peak positions $\pm H_p$ of the MHL curve there exists a threshold value E_c (and associated with it, a critical sweep rate) for which the E-J characteristic is non-power-law. On the other hand, for any $|H_a^{\perp}| > |H_p|$, the linearity in the E-J dependence on a log-log scale is preserved. Moreover, the slope is the same as when no in-plane field is present. We will come back to this
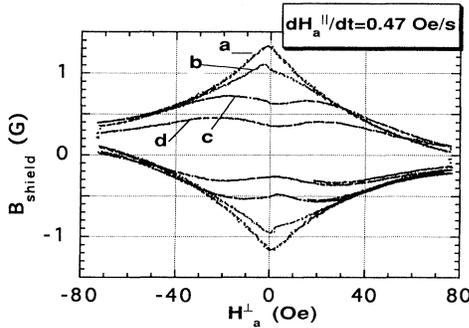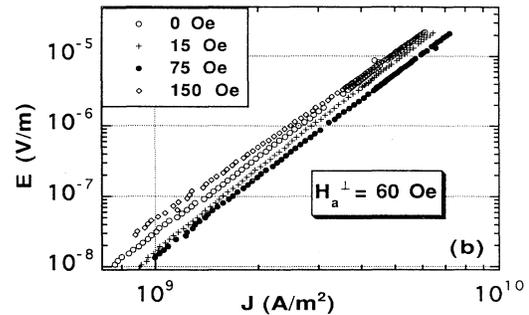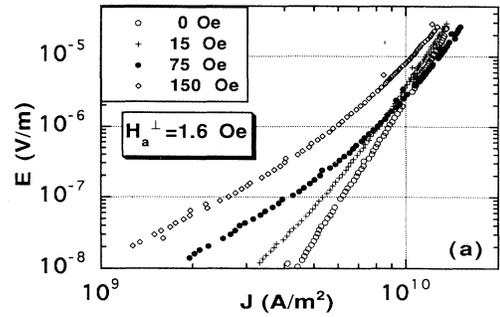

FIG. 6. EJ curves extracted from variable sweep rate magnetization data at four different in-plane applied fields $H_a^{\parallel}$: (a) $H_a^{\perp}$=1.6 Oe and (b) $H_a^{\perp}$=60 Oe.

peculiarity in the next section.

Although the E-J results are for a limited range of electric fields, we attempted this analysis in order to determine the change of the form of the pinning potential and its value. A general form[36] for the activation energy introduces a parameter μ which serves to identify different dissipation mechanisms:

$$U(j) = \frac{U_0}{\mu}\left[\left(\frac{j_c}{j}\right)^{\mu} - 1\right] \qquad (2)$$

contains Zeldov et al.'s model[31] ($\mu = 0$), the collective creep/vortex glass model ($0 < \mu \le 1$),[37-39] and recovers the classic Anderson-Kim picture[40] of linear $U(j)$ for $\mu = -1$.

FIG. 5. Magnetization curves at sweep rate of 0.47 Oe/s and four different in-plane applied fields: 0 (curve a), 15 (curve b), 75 (curve c), and 150 (curve d) Oe.
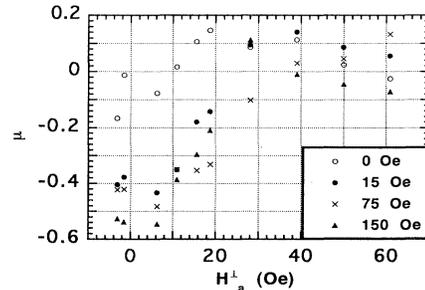

FIG. 7. Perpendicular field dependence of the exponent μ extracted from the EJ characteristics at four different in-plane applied fields $H_a^{\parallel}$.

We extracted the exponent μ from the E-J characteristics by taking the slope of $\ln\left[\frac{\partial\ln E}{\partial j}\right]$ vs $\ln(j)$ which is equal to $-(\mu+1)$. As expected at large angles, $\mu \approx 0$, corresponding to power law behavior, for all in-plane fields (see Fig. 7). At small angles, if the in-plane field is present, μ tends to go to -1 signaling creep enhancement and weaker pinning.

Similar anomalous magnetization results have also been obtained on a 0.5%-Zn-doped (substitution for Cu) BSCCO film.

DISCUSSION

A possible phenomenological explanation of the observed dependence of the critical current density j_c on $\vec{H}_a^{\text{tot}}$ lies in the dimensionality of the vortex lattice state in BSCCO in this region of the H-T space as well as in the form and strength of the pinning disorder. The interplay between several interactions and length scales determines the final form of the vortex lattice: inter- and intraplane vortex pancake coupling, strength and range of the pinning forces exerted on the vortex structure by the crystal lattice defects, as well as the forces exerted by the in-plane shielding currents. The detailed knowledge of all these interactions is hard to establish but some approximations can always be made and reasonable conclusions drawn.

The characterization of pinning defects in the BSCCO films and their relative strength is a formidable task. Wagner et al.[41] analyzed the possible origins and forms of pinning centers present in BSCCO films, and, although no conclusive answer was given for all of them, it is clear that point oxygen vacancies are inevitable defects. They provide the major pinning source since their density and, more important, their density *fluctuation* is much higher. The pinning potential strength is greatly reduced at these temperatures by thermal fluctuations:

$$U_c = \frac{U_{c0}}{\left(1 + \frac{\langle u^2 \rangle_{\text{th}}}{\xi_{ab}^2}\right)^{1/2}} \; . \qquad (3)$$

If the vortex line tension is strong enough to keep the finite correlation of vortex pancakes in the $\hat{c}$ direction in place, but weak enough to enable the vortex lines to adjust to the pinning center density fluctuation in each plane, we can expect a finite correlation length along the field direction L_c larger than the interlayer spacing d and a finite critical current density j_c. On the other hand, if $L_c < d$ the 2D pinning of decoupled vortex pancakes will be established.

As we pointed out earlier, all our measurements are performed at low magnetic fields, in the limit where $\lambda_{ab} \lesssim a_0$. This brings us to the dilute vortex line or pancake limit, but in order to establish which regime of collective pinning is appropriate in this case one has to compare the intervortex distance a_0 with the correlation length along the field direction L_c using the scaling relationship for the anisotropic case.[42] If

$$L_c^c < a_0/(\gamma\sqrt{\varepsilon_\theta}) \qquad (4)$$

holds, then according to the theory[42] we should be in the single vortex pinning regime [here $L_c^c = L_c(\theta)\varepsilon_\theta$ is the vortex correlation length for a field applied along the $\hat{c}$ direction and $\varepsilon_\theta = \gamma^{-2}\cos\theta^2 + \sin\theta^2$ is the angular-dependent anisotropy parameter]. Direct estimates of L_c from the critical current value[42] $L_c = (\xi_{ab}/\gamma)(j_0/j_c)^{(1/2)} \approx 0.6$ nm suggest a pure 2D picture in this case, due to the fact that $L_c < d \approx 1.5$ nm, where $j_0 \approx c\Phi_0/(12\sqrt{3}\pi\lambda^2\xi) \approx 6\times10^7$ A/cm^2 is the estimated depairing current for BSCCO and $\gamma \approx 50$. On the other hand, if we assume that the limit of vortex bundle pinning (either small or large vortex bundles) is appropriate, the inequality (4) should be reversed, thus bringing L_c^c significantly above the interlayer distance d.

As long as the interlayer vortex coupling length exceeds d, two possibilities can occur depending on the ratio of L_c^c/t, where t is the film thickness. If this ratio is less than 1 the vortex structure will be three dimensional and the critical current's angular dependence on the applied magnetic field will not simply scale with $H_a^\perp$ but will depend on the in-plane component $H_a^\parallel$, too. If, on the other hand, the correlation length exceeds the film thickness, the critical current behavior will retain its two-dimensional dependence and scale with $H_a^\perp$.[42]

Our experimental results show 2D behavior at large $H_a^\perp$. The form of the MHL's at the same sweep rate, but different $H_a^\parallel$, is very similar in this region (Fig. 4). Moreover, the E-J curves extracted at various $H_a^\parallel$ have identical slopes on a log-log scale if the field component $H_a^\perp$ is the same (Fig. 6). Two possible conclusions can be drawn from this result: two-dimensionality is either due to completely decoupled layers in BSCCO leading to correlation lengths smaller than d, or the correlation length along the field is larger than the effective film thickness $t_{\text{eff}} = t/\sin\Theta$. In either case the single vortex collective pinning theory for anisotropic superconductors does not allow for a dimensional crossover because the ratio $L_c(\Theta)/t_{\text{eff}}$ remains the same for all angles $\Theta \gg \gamma^{-1}$. If the magnetic system is completely decoupled there should be no significant change in the MHL shape with the application of in-plane field at any $H_a^\perp$ at the same sweep rate, except very near $H_a^\perp=0$ where self-fields or surface barriers may cause deviations (as mentioned, the lock-in transition is ruled out in this experiment). As can be seen from Fig. 4 a significant departure from the MHL with $H_a^\parallel=0$ occurs with increasing $H_a^\parallel$. The deviation covers a range of $H_a^\perp$ reaching to about $\mu_0 H_a^\perp = 60$ G for the largest in-plane field which is 4–5 times larger than the calculated self-field. This clearly shows that the assumption of 2D due to completely decoupled layers does not hold. Turning to the second possible explanation, we postulate that at large tilting angles Θ (large $H_a^\perp$) the correlation distance along the magnetic field is larger than the film thickness t and the in-plane critical current density scales with $H_a^\perp$. There are significant differences between the above two cases. One of them is the fact that the penetration of the tilted vortices with finite "length" has well defined anisotropies of penetration

as discussed by Brandt.[43] This effect deals with the fact that for tilted applied magnetic fields vortex line motion perpendicular to the c axis becomes highly anisotropic. The viscosity for vortex movement perpendicular to the $\hat{B}\hat{c}$ plane becomes much smaller than for the movement along the plane. Viscosities scale as $\eta^{\perp} = \eta_c \sin\Theta$ and $\eta^{\parallel} = \eta_c / \sin\Theta$, respectively, for the case of $\Theta \gg \gamma^{-1}$, where η_c is the flux line viscosity for the case when $\hat{B} \parallel \hat{c}$. Thus at relatively small Θ enhanced anisotropic creep will cause a rapid decrease of the trapped flux as well as its entry, depending on the measurement history.

The measurable onset of the anisotropic penetration will directly depend on the characteristic diffusion times of vortices into the superconductor and consequently the applied field sweep rate. Since the anisotropy in diffusion scales as $\sin^2\Theta$ angles between the $\vec{H}_a^{\text{tot}}$ and ab plane of less than $20°$–$25°$ should cause significant deviations in $j(H_a^{\perp})$ curves. This analysis neglects the effect of field gradients in the sample as well as boundary effects. The actual angle of the vortex lines will be corrected by the local self-field, which in the case of our film does not exceed 10–15 G. Since the film thickness is of the order of the in-plane penetration depth the surface effects might be significant.[43] Summarizing, the actual angle of the vortex lines with the ab plane will not be equal to the angle of $\vec{H}_a^{\text{tot}}$ and will vary across the disk area. The deviations should be more pronounced at high sweep rates due to stronger field modulation.

The analysis of the experiment is consistent with the above estimates. The creep enhancement near $H_a^{\perp}=0$ Oe is barely noticeable at small in-plane fields due to comparable self-field even for the lowest available sweep rates. In this case the angle between the vortex lines and the ab plane remains large for any $H_a^{\perp}$. When larger in-plane fields are applied, the anomaly is first evident as a small kink in magnetization near $H_a^{\perp}=0$ Oe, developing into a minimum as the sweep rate is further decreased. At low sweep rates, the film is in a more relaxed state and $\vec{B}_{\text{shield}}$ is more uniformly distributed across the film area. In addition the time scale of the measurement is effectively increased in this case, enabling us to integrate out larger changes of magnetic flux. This implies that the peaks in the MHL curve should be spaced further apart and be more abrupt towards $H_a^{\perp}=0$ with the decrease of the sweep rate, as we observe (Fig. 8). It also confirms the idea that the process is not instantaneous over the disk area but rather propagates during the field rotation.

Finally, we mention recent experimental observations which might be associated with our results. Two types of barriers for flux penetration into the superconductor have been frequently discussed: geometrical, and surface edge (Bean-Livingston) barriers. Zeldov et al.[44,45] have recently analyzed the influence of a geometric barrier on the irreversibility line and its contribution to the irreversibility in magnetization at low magnetic fields in BSCCO.[45] The asymmetric peaks near zero field observed in BSCCO single crystals were consistently explained as being due to delayed entrance of vortices when the field direction is reversed. In our geometry we would expect strong peaks to be located very close to $H_a^{\perp} = 0$ separated by a field
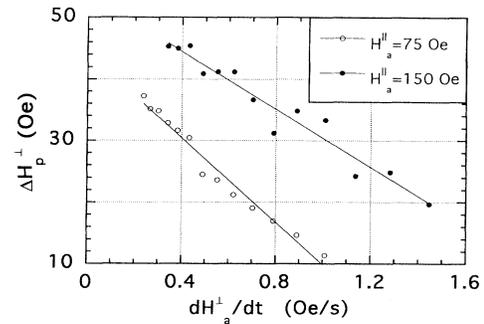

FIG. 8. Sweep-rate dependence of the distance between the peaks in magnetization at two different in-plane applied fields $H_a^{\parallel}$.

on the order of $H_{c1}(T)(d/W)^{1/2}$ (the exact formula was derived for a strip geometry only with thickness d and width W) $\approx 0.01 H_{c1}(77\text{K}) \approx 0.3$ G. Clearly this is not the case in our experiment: first, the peaks are symmetric with respect to the center of the magnetization curve and, second, the maxima in magnetization are separated by fields up to about 20 G with an approximately linear dependence on the sweep rate. An effect of geometrical origin cannot explain the dependence on the magnitude of the in-plane applied field or on the sweep rate. Edge barriers, extensively studied[46,47] and observed by several authors,[5] are out of the question for all the reasons stated above and also because our wet-etched samples have an inhomogeneous edge morphology on the order of 2 μm, which effectively destroys the Bean-Livingston barrier. Such a barrier would also not produce significant changes with sweep rate.

The closest approach to ours was that taken by Indenbom et al.,[19] who used Faraday effect imaging to observe the penetration of the perpendicular flux in the presence of an in-plane applied magnetic field. They interpret anisotropy in penetration as evidence of the three-dimensional nature of vortex lines based on the same analysis given by Brandt.[43] They present evidence for three-dimensionality in YBa$_2$Cu$_3$O$_{7-\delta}$ YBCO crytals and a somewhat reduced effect in YBCO films; in contrast to our results, they do not register it in BSCCO. From this they conclude that vortex structure in BSCCO is completely decoupled between the layers, i.e., consists of 2D vortex pancakes. It is not clear why the effect was not observed in their experiment, although possible reasons could be its sweep-rate dependence and temperature. Lower temperatures should enhance the pinning, causing larger effective times for hopping as well as smearing of the anisotropy.

CONCLUSION

We have presented evidence for a three-dimensional vortex behavior in as-grown Bi$_2$Sr$_2$CaCu$_2$O$_{8+\delta}$ thin films at 77 K. Strong enhancement of the perpendicular field component's creep rate in the presence of an in-plane applied magnetic field clearly indicates a 3D behavior.

This finding is in line with the theory by Glazman and Koshelev,[16] according to which at magnetic fields below B_{cr} the vortex system in BSCCO consists of well correlated vortex lines rather than layers of decoupled vortex pancakes. This experiment confirms the similar recent findings on $Bi_2Sr_2CaCu_2O_{8+\delta}$ single crystals with introduced columnar defects[21,22] and shows that this behavior is intrinsic to HTS BSCCO materials. Further temperature-dependent studies of the effect as well as its possible existence in model systems might give additional insight into the dynamics of the vortex state in layered HTS materials.

ACKNOWLEDGMENTS

APPENDIX

Generation of "contactless current-voltage characteristics" from magnetization measurements has been discussed in the literature,[24,26] and here we present the method applied to the present experiment: a magnetic field whose rate of change is constant, applied to a superconducting disk. We assume a constant shielding current $\vec{J}_{shield}$ across the film area and prove the validity of this assumption.

We treat the disk as a series of concentric superconducting rings coupled inductively to one another. If the current density is constant throughout the disk, it is easy to calculate the field generated. The measured field therefore directly determines the current density using the well known expression.[48] The determination of the voltage is more complicated. We begin with the differential equation that describes the concentric currents in
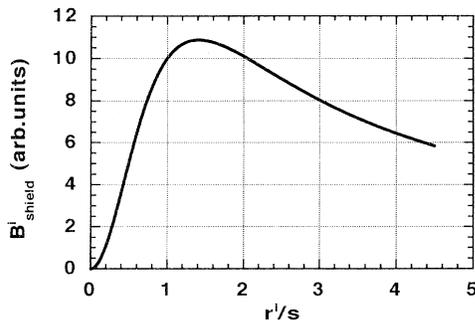
FIG. 9. Relative contribution of the ith current ring with radius r^i to the total magnetic field measured by the Hall probe at distance s from the film's plane.
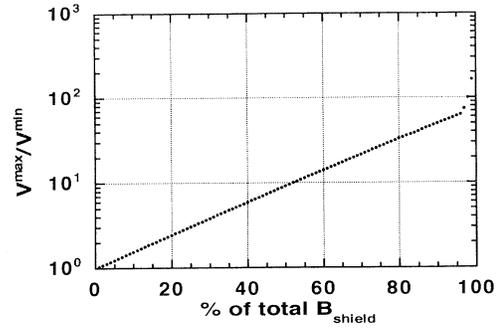
FIG. 10. Relative electric field variation across the disk (ring) as a function of the relative magnetic field measured by the Hall probe.

each ring as the magnetic field $H_a^\perp$ is applied with a sweep rate $dH_a^\perp/dt$:

$$\frac{d\Phi_{ext}^i}{dt} + \frac{d\Phi_{int}^i}{dt} = -V_{emf}^i. \qquad (A1)$$

The external flux in the ith ring comes from the spatially uniform applied field and is $\Phi_{ext}^i = H_a^\perp S^i$ where S^i is the area of ring i. Its time derivative is directly obtained from the sweep rate. The internal flux in the ith ring due to currents in all the rings is $\Phi_{int}^i = \sum_k L_{ik} I_k$ where I_k is the current in the kth ring and L_{ik} is the mutual inductance between the ith and kth rings (for $i \neq k$) or the self-inductance of the ring (for $i = k$). The inductances were calculated from the formulas in Ref. 49. The time derivative of the current is obtained from the sweep rate of the perpendicular applied field and the slope of the $M(H_a^\perp)$ curve [which is, in effect, $I_{shield}(H_a^\perp)$] via

$$\frac{dI_{shield}}{dt} = \frac{dI_{shield}}{dH_a^\perp}\frac{dH_a^\perp}{dt}. \qquad (A2)$$

Equations (A1) and (A2) determine the voltage V_{emf}^i in the ith ring. It is clear that the voltage is not the same for each ring; indeed, the span of voltages can be several decades. However, if we are willing to settle for a less precise knowledge of the total current, we can discard those rings which give the lowest contribution to the magnetic field measured by the probe. This effectively narrows the voltage spread. Figure 9 shows the relative contribution from each ring of radius r^i to the total magnetic field from the disk measured by the Hall probe at the location in this experiment. We eliminate the rings with the lowest contribution and compare the amount of the field measured by the probe relative to that seen when the disk is complete. If we label the calculated emf in the ring with the largest radius V_{emf}^{max} and the one with the smallest radius V_{emf}^{min}, the ratio of these two values gives a relative voltage spread (Fig. 10). In the case of 5% field accuracy, $\frac{V_{emf}^{max}}{V_{emf}^{min}} \approx 60$ which corresponds to $\frac{E_{emf}^{max}}{E_{emf}^{min}} \lesssim 8$. As evident from Fig. 6 the current does not change substantially over less than one decade of electric field. This shows that the approximation of a constant shielding current $\vec{J}_{shield}$ throughout the disk area is a valid one.

[1] J. Clem, Phys. Rev. B **43**, 7837 (1991).

[2] P. H. Kes, J. Aarts, V. M. Vinokur, and C. J. van der Beek, Phys. Rev. Lett. **64**, 1063 (1990).

[3] I. Felner *et al.*, Physica C **162-164**, 1635 (1989).

[4] D. Farrell *et al.*, Phys. Rev. Lett. **63**, 782 (1989).

[5] W. R. White, Ph.D. thesis, Stanford University, 1994, Chap. 3.

[6] A. Buzdin and A. Simonov, Sov. Phys. JETP **71**, 1165 (1990).

[7] A. Grishin, A. Martynovich, and S. Yampol'skii, Sov. Phys. JETP **70**, 1089 (1990).

[8] A. Koshelev, Phys. Rev. B **48**, 1180 (1993).

[9] P. Gammel, D. Bishop, J. Rice, and D. Ginsberg, Phys. Rev. Lett. **68**, 3343 (1992).

[10] L. Gurevich *et al.*, Physica C **195**, 323 (1992).

[11] D. Feinberg and C. Villard, Phys. Rev. Lett. **65**, 919 (1990).

[12] L. Bulaevskii, M. Ledvij, and V. Kogan, Phys. Rev. B **46**, 366 (1992).

[13] A. Vermeer *et al.*, Physica C **185-189**, 2345 (1991).

[14] F. Steinmeyer *et al.*, Europhys. Lett. **25**, 459 (1994).

[15] M. Oussena, P. A. J. de Groot, R. Gagnon, and L. Taillefer, Phys. Rev. Lett. **72**, 3606 (1994).

[16] L. Glazman and A. Koshelev, Phys. Rev. B **43**, 2835 (1991).

[17] H. Arribere *et al.*, Phys. Rev. B **48**, 7486 (1993).

[18] H. Safar *et al.*, Phys. Rev. B **46**, 14 238 (1992).

[19] M. Indenbom *et al.*, Physica C **226**, 325 (1994).

[20] D. Grier *et al.*, Phys. Rev. Lett. **66**, 2270 (1991).

[21] L. Klein *et al.*, Phys. Rev. B **48**, 3523 (1993).

[22] C. van der Beek *et al.*, Phys. Rev. Lett. **74**, 1214 (1995).

[23] P. Wagner *et al.*, Physica C **215**, 123 (1993).

[24] W. Paul and T. Baumann, Physica C **175**, 102 (1991).

[25] W. Paul and J. P. Meier, Physica C **205**, 240 (1993).

[26] M. Polk *et al.*, Physica C **174**, 14 (1991).

[27] G. Ravi Kumar and P. Chaddah, Phys. Rev. B **39**, 4704 (1989).

[28] W. Fietz, M. Beasley, J. Silcox, and W. Webb, Phys. Rev. **136**, A335 (1964).

[29] S. Senoussi, M. Oussena, G. Collin, and I. Campbell, Phys. Rev. B **37**, 9792 (1988).

[30] J. Pearl, Appl. Phys. Lett. **5**, 65 (1964).

[31] E. Zeldov *et al.*, Appl. Phys. Lett. **56**, 680 (1990).

[32] H. Dowes and P. Kes, J. Alloys Compounds **195**, 451 (1993).

[33] S. Maslov and V. Pokrovsky, Europhys. Lett. **14**, 591 (1991).

[34] M. Daeumling, J. Seuntjens, and D. Larbalestier, Nature **346**, 332 (1991).

[35] L. Klein *et al.*, Europhys. Lett. **14**, 591 (1991).

[36] H. Schnack *et al.*, Physica C **197**, 337 (1992).

[37] M. Feigel'man, V. Geshkenbein, and A. Larkin, Physica C **167**, 177 (1990).

[38] V. Vinokur, P. Kes, and A. Koshelev, Physica C **168**, 29 (1990).

[39] D. Fisher, M. Fisher, and D. Huse, Phys. Rev. B **43**, 130 (1991).

[40] P. Anderson and Y. Kim, Rev. Mod. Phys. **36**, 39 (1964).

[41] P. Wagner, F. Hillmer, U. Frey, and H. Adrian, Phys. Rev. B **49**, 13 184 (1994).

[42] G. Blatter *et al.*, Rev. Mod. Phys. **66**, 1125 (1994).

[43] E. Brandt, Phys. Rev. Lett. **68**, 3769 (1992).

[44] E. Zeldov *et al.*, Phys. Rev. Lett. **73**, 1428 (1994).

[45] E. Zeldov *et al.* (unpublished).

[46] A. Koshelev, Physica C **223**, 276 (1994).

[47] L. Burlachkov, Physica B **194-196**, 1821 (1994).

[48] L. Landau and E. Lifshitz, *Electrodynamics of Continuum Media*, Course of Theoretical Physics Vol. 8 (Pergamon Press, Oxford, 1984).

[49] F. W. Grover, *Inductance Calculations, Working Formulas and Tables* (Instrument Society of America, Research Triangle Park, NC, 1981).
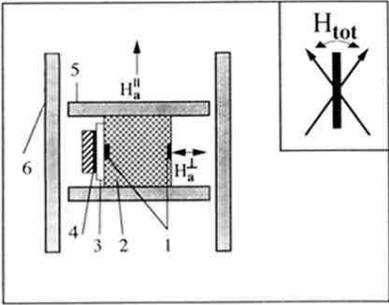
FIG. 1. Experimental setup: InSb Hall probes (1), sapphire sample holder (2), 0.5-mm MgO spacer (3), thin-film BSCCO disk (4), and a set of perpendicular solenoids (5,6).